

# Research Project in Mechatronics Engineering

---

Literature Review

## Variable Arm Angle and Control Modification for Multi-rotor UAVs

Oliver Reedy

Project Report ME036-2024

---

Co-worker: James Blackhurst

Supervisor: Dr Shahab Kazemi

Co-Supervisor: A. Prof Karl Stol

13 October 2024



**ENGINEERING**  
DEPARTMENT OF MECHANICAL  
AND MECHATRONICS ENGINEERING

## **VARIABLE ARM ANGLE AND CONTROL MODIFICATION FOR MULTI-ROTOR UAVS**

**Oliver Reedy**

### **ABSTRACT**

This report presents the designing, manufacturing, and physical testing of a variable arm modification for a multi-rotor Unmanned Aerial Vehicle (UAV).

The report begins with an investigation into existing actuated control mechanisms modified to be attached to UAVs, along with their associated control systems. A key takeaway observed is ensuring the mechanism induces minimal force upon the body of the UAV itself, by reducing weight and ensuring centre of gravity (CoG) remains stationary.

A mechanism involving a central position controlled gear is settled on as the design as to ensure that while no end-effector is attached, the CoG remains in-line with the centre of the UAVs geometry.

The key attributes of the design and assembly are discussed, including material selection and building methods. The pipeline allowing an Off-board Simulink controller to position the angle of the arm is discussed.

A mechanism capable of rotating and maintaining flight stability whilst in motion is successfully constructed and tested, showcasing feasibility and potential for future works.

The relation between the weight of an end-effector, the velocity it undergoes, and the resulting deviations in pitch and position control are investigated. The reasons underpinning the relationships are discussed. The decrease in flight stability and increase in correlation between pitch error and arm velocity as end-effector mass increases is highlighted.

Future work may introduce use of the motor encoder count and velocity into the control system to counteract the deviation in position error during arm rotation. Expanding the experiments to involve physical interaction is key to fully utilise the full potential and desired application of the mechanism.

## DECLARATION


### Student

I Oliver Reedy ..... hereby declare that:

1. This report is the result of the final year project work carried out by my project partner (see cover page) and I under the guidance of our supervisor (see cover page) in the 2024 academic year at the Department of Mechanical Engineering, Faculty of Engineering, University of Auckland.
2. This report is not the outcome of work done previously.
3. This report is not the outcome of work done in collaboration, except that with a project sponsor as stated in the text.
4. This report is not the same as any report, thesis, conference article or journal paper, or any other publication or unpublished work in any format.

In the case of a continuing project: State clearly what has been developed during the project and what was available from previous year(s):

1. Variable Arm Mechanism was designed, built, attached and experimentally tested by us, but the drone itself was provided by the DTRG, having been developed by a previous PhD student, and utilized in prior P4Ps.
2. Simulink and PX4 code were available from previous works and utilized in this project with no major alterations.

Signature: 

Date: 09/10/2024

### Supervisor

I confirm that the project work undertaken by this student in the 2024 academic year **is** / ~~is not~~ (*strikethrough as appropriate*) part of a continuing project, components of which have been completed previously.

Comments, if any:

Signature: 

Date: 10/10/2024

# Table of Contents

<b>Acknowledgements</b>	<b>vi</b>
<b>Glossary of Terms</b>	<b>vii</b>
<b>Abbreviations</b>	<b>vii</b>
<b>1 Introduction</b>	<b>1</b>
1.1 Research Objects	1
1.2 Scope	2
<b>2 Literature Review</b>	<b>2</b>
2.1 Articulated Arm Configurations attached to UAVs	2
2.2 Control Systems of UAVs with Interactions Devices	4
2.3 Conclusion	6
<b>3 Designs and Methods</b>	<b>7</b>
3.1 Design Considerations	7
3.1.1 Initial UAV Specifications	7
3.1.2 Initial Design Considerations	7
3.2 Mechanical Design	8
3.2.1 Design of Rotating Mechanism	8
3.2.2 Material and Manufacturing Method Considerations	9
3.2.3 Initial Prototype Assembly	10
3.3 Prototype Testing and Iteration	10
3.3.1 Testing Process	10
3.3.2 Iteration Process	10
3.3.3 Finalised Physical Prototype	11
3.4 Actuator and Code Design	12
3.4.1 Dynamixel Setup	12
3.4.2 Off-board Simulink Control	13
3.4.3 Dynamixel Troubleshooting	14
3.4.4 Validating Flight System	14
<b>4 Experiments and Data Processing</b>	<b>16</b>
4.1 Experiment Setup and Process	16
4.2 Issues Faced During Experimentation	16
4.2.1 Weight Limits	16
4.2.2 Flight Control	17
4.2.3 Battery Drainage and Actuator Saturation	17
4.3 Parsing of Data	17
4.3.1 Data Logs	17
4.3.2 Vicon Data	17
4.3.3 Overlaying Data	17
<b>5 Results and Discussion</b>	<b>18</b>
5.1 No End-Effector Mass Installed	18
5.2 Increasing Mass Installed on End-Effector	20
5.3 OhmStick Installed on End-Effector	23
<b>6 Conclusions and Future Works</b>	<b>24</b>

6.1	Conclusions . . . . .	24
6.2	Future Works . . . . .	25
	<b>References . . . . .</b>	<b>25</b>

## **Acknowledgements**

Without the help of the fantastic people at the University, this project would not have been possible.

To Dr Shahab Kazemi, for his invaluable guidance and presence throughout the year, and without which this project would not have been possible.

To the amazing Mechanical/Mechatronics community, Chantelle, and Salim, for lending their help and knowledge when we needed it most.

And to James, the best project partner I could have hoped for.

## Glossary of Terms

Altitude	Distance above ground
Armed	UAV state where flight is ready to be directly engaged
Attitude	Object's orientation with respect to inertial frame
Body Frame	Coordinate system which moves with reference to body of drone
Disarmed	UAV state where multi-rotor is powered but motors are not powered
Drone	Interchangeable with UAV in the context of this report
End-Effector	A device attached to the end of a robotic appendage
Inertial Frame	Fixed coordinate system used as a reference for the motion of objects
MATLAB	Software with a programming and numeric computing environment
MAVLink	Protocol for intercommunication between UAVs and computers
Multi-rotor	Rotor-craft with more than two lift generating rotors
Pitch	Lateral axis rotation, tilt of a drone forwards or backwards
QGroundControl	Software providing full flight control and mission planning for any MAVLink enabled drone
Roll	Longitudinal axis rotation, tilt of a drone side-to-side
Rotor	An actuator that drives propellers to produce lift and control movement on a UAV
Simulink	A simulation toolbox, available as a MATLAB add-on
Vicon	Motion capture system in Motion Capture Lab, capable of tracking reflective markers using camera system.
Yaw	Vertical axis rotation, turning of a drone left or right

## Abbreviations

3D	Three Dimensional
CoG	Centre of Gravity
DoF	Degrees of Freedom
DTRG	Drone Technology Research Group
PID	Proportional - Integral - Derivative
PX4	PixHawk 4
TTL	Transistor-Transistor Logic
UAV	Unmanned Aerial Vehicle
UDP	User Datagram Protocol

# 1. Introduction

Drones, in particular multi-rotor Unmanned Aerial Vehicles (UAVs), have rapidly developed across the last few decades. Advances in drone components, including microprocessors, high-energy lithium polymer batteries, micro electro-mechanical systems sensors, and efficient actuators have all fuelled these developments [1]. Drones are now present across a huge range of applications. From industrial site management [2], crop monitoring [3], to military operations. Drone technology will continue to increase in popularity and functionality.

The University of Auckland's Drone Technology Research Group (DTRG) is where researching future applications of drones occurs at the University. Backed by the Ministry of Business, Innovation, and Employment, the focus is on the control and performance of drones for real-world applications and challenges. Of interest is the study of physical interaction with the environment while in flight. For example, connecting to power line in order to perform inspections safely [4].

The most common type of UAV is an under-actuated quad-copter, which utilises 4 rotors to achieve flight. Movement in the horizontal plane requires the use roll or pitch, with rotation being controlled by the yaw. This limitation has given way to the use of over-actuated UAV for the purposes of many of the DTRG's projects. Fully-actuated UAVs require 6 actuators to account for the 6 degrees of freedom (DoF) present for unconstrained movement in three dimensional (3D) space. Over-actuated UAVs incorporate additional redundancy motors dependant on the desired design. Configurations examples include variable-tilt rotors and variable-tilt rotor blades, but the configuration utilised by DTRG is a fixed tilt over-actuated UAV. With the use of a non-parallel arrangement of 8 actuators, similar to a mecanum wheel setup seen in omni-directional rovers, movement can be achieved in the horizontal plane without the use of roll or pitch. This is done by maintaining the vertical balance of forces with the motors whilst favouring the motors which tilt in the desired directional. Using this in conjunction with regular quad-copter dynamics, by treating vertically paired actuators as the single actuators present in a quad-copter, any individual axis can be translated upon or rotated about without infringing on the others.

This project aims to develop a rotating arm attached to an over-actuated UAV, before designing a control system which will alter the control gains based on the real-time angle of the arm, and maintain stability whilst the UAV is in free-flight or physically attached via the arm.

## 1.1 Research Objects

The research objects are as follows:

- Determine an ideal and feasible configuration for the manipulable arm, and the mechanisms behind it's function.
- Design, manufacture, and test the variable arm. Alter the frame of the provided UAV to support the arm, and allow for flight and experimentation.
- Develop a control system that can maintain stability whilst moving the arm in free-flight, and during an attached period, and experimentally evaluate it to improve and determine success.

- Develop a framework for continuation of project (e.g gripping device, additional DoF, physical application).

As the project continues, these overarching research and project goals will be broken down into smaller sub-research goals, such as determining the best materials, gains, type of control system, and so on.

## **1.2 Scope**

The scope is as follows:

- Designing and building the arm and the mechanisms required to ensure it functions, whilst maintaining restrictions required to ensure flight is possible, such as size and weight.
- Altering the PixHawk firmware to support a custom control system, and interfacing with Simulink to allow for controlled flight.
- Experimentally testing the UAV with the MoCap studio vision system, using experiments designed to quantify the UAVs ability.

Out of scope is as follows:

- Designing and building a new UAV.
- Adding additional DoF within the arm.
- Sensing equipment incorporated into the control system.
- Camera / external sensor integration.

## **2. Literature Review**

### **2.1 Articulated Arm Configurations attached to UAVs**

In this section research performed into articulated arm configurations for UAVs will be discussed, with particular attention to the capabilities of the modifications, and the actuators they use.

Wegrowski et al. [5] analysed a prototype robotic arm for a quad-copter which incorporated a bottom mounted folding arm design. The folding arm design was chosen so that during regular flight operation the arm could be retracted to prevent unnecessary danger and increase stability. It was found with use of a single actuator, light-weight materials, and heavy constraints on the arm movement, a successful prototype could be made.

Ollervides-Vazquez et al. [6] opted for a conceptual approach. Simulations were performed on an octo-copter UAV with an under-mounted 3 DoF manipulator arm seen in Figure 1. The octo-copter's robust propeller system allows it to carry a maximum load capacity of 16kg, consequently allowing for the heavily actuated arm component. The calculations, simulations, and findings from the paper will become more relevant in the control systems section.

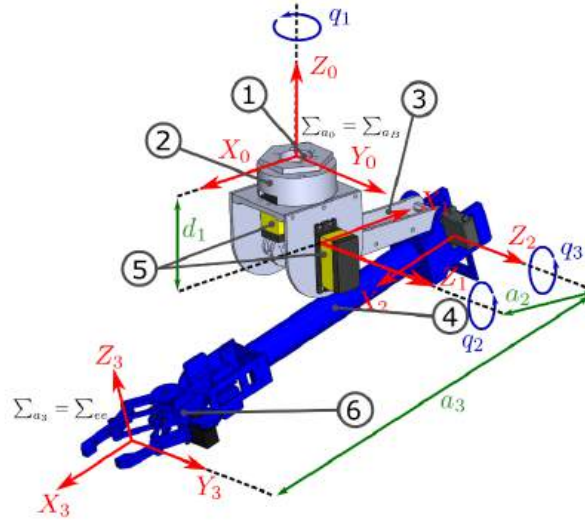


**Figure 1** Image of the manipulator arm attached to an octo-copter

Suthar and Jung's [7] approach to an aerial manipulator arm was similar to Wegrowski et al. [5], incorporating foldable robotic arm for drones (FRAD), with the addition of a twisting-string actuator (TSA) seen in Figure 2. This provides an additional DoF to the manipulator in the form of a rotation around the z-axis. The TSA-based FRAD was able to lift payloads of 0.3kg, achieving the designed mechanism weight-to-payload ratios required for successful drone flight. Although not tested in conjunction with drone flight, inspiration for novel articulated controllers can be drawn.

IEEE ROBOTICS AND AUTOMATION LETTERS, VOL. 6, NO. 3, JULY 2021

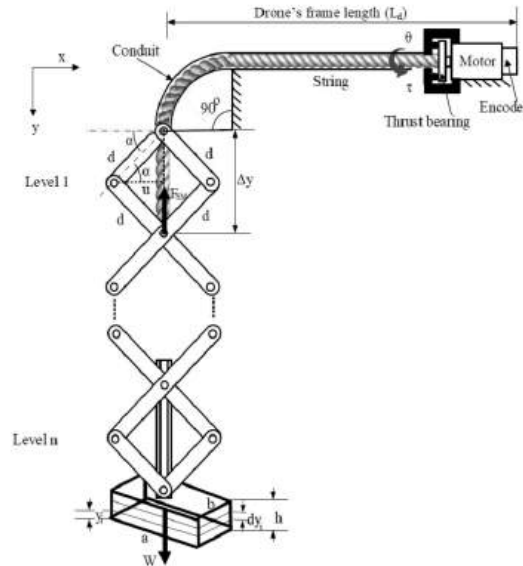


**Figure 2** Twisting-String Actuator with Scissor Arm Mechanism attached [7].

Many of the existing examples follow the trend of taking a standard robotic arm design and slightly modifying it to work with drone. However, a paper 2018 instead incorporates the mechanism of the manipulator into the body of the drone itself in some of the showcased designs. Their multi-directional thrust octo-rotor with an inspection arm, named AeroX, achieves 6 DoF in the inspection arm which rotates about the body of the drone itself, as seen in Figure 3 [8].



**Figure 3** AeroX, a multi-directional thrust octo-rotor with an inspection arm [8]

The AeroX design was expanded upon the next year, in 2019 with Trujillo et al. [9]. The octo-copter design was optimised. The design of the arm is showcased in Figure 4. Without the aid of any drone movements, the end-effector on the arm is able to achieve 6 DoF and precise position control.

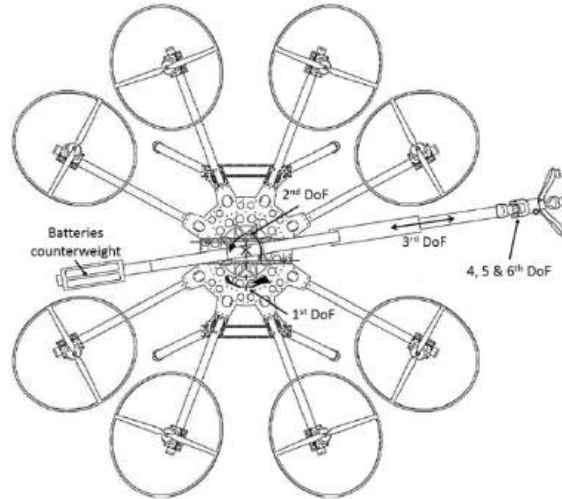


**Figure 4** Design of AeroX showcasing DoF in arm [9]

## 2.2 Control Systems of UAVs with Interactions Devices

Although the ultimate choice of configuration for the interaction device is instrumental in the overall project, the attached control system is often the deciding factor of its success. In this section, numerous control systems used with aerial arm manipulators will be discussed.

Returning to Ollervides-Vazquez et al. [6], the approach to the dynamics and combined control system used provides an ideal way to approach a simulation based setup. Classical Denavit-Hartenberg convention was used to acquire the kinematics of their octo-copter drone, and the recursive Newton-Euler method was used to acquire the dynamics model. A cascade PID controller was then applied to the navigation and attitude of the UAV, with a simple PID controller on the manipulator arm. The simulations showed the moments applied from the arm would induce disturbance effects on the navigation tracking trajectory, whilst translation and orientation movements of the UAV would induce disturbances into the joint position control..

Muscio et al. [10] suggest an alternate approach to the control system of a combined UAV

and manipulator arm. A 3-layer control architecture for multiple aerial robotic manipulators is used. The top layer determines the end-effector desired trajectory for each manipulator deciding what each arm should do. The middle layer is local to each vehicle, and computes the motion references needed to track the effector trajectories, with the bottom layer being used to compute the aforementioned motion references, calculate the dynamics, and apply the signals to the actuator. Although the system is geared towards larger, complex systems with multiple manipulator arms, the general architecture is highly adaptable; applying it to an alternate design would be trivial.

A multi-layer control for a UAVs equipped with a servo robot arm is proposed in Ruggiero et al. [11]. The control system can be seen in Figure 5. The first step involves a novel mechanism which makes use of the drone battery as the counterweight for the statics of the robotic appendage. The residual effects from the internal dynamics whilst moving the arm are computed and compensated using the UAVs thrust and torque abilities. The last layer involves estimating the moments acting on the aerial vehicle and feeding the estimations into the controller and a disturbance feedback loop. The final system was experimentally proven to be viable and applicable to any sort of UAV configuration.

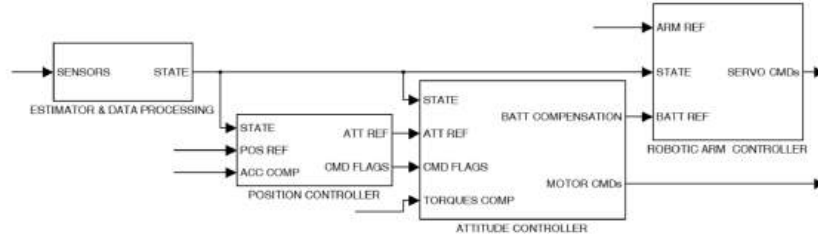


**Figure 5** Multi-layer control system. Ruggiero et al. [11]

Another multi-layer control system is proposed by Cataldi et al. [12] in their impedance control of an aerial-manipulator, which shares some similarities to the control system proposed by Muscio et al. [10]. The proposed control system consists an outer loop composed of a trajectory generator combined with an impedance filter, as showcased in Figure 6. This results in compliant movement in the end-effector space. The middle loop uses inverse kinematics to generate the joint space variables. The inner loop is used to ensure the motion tracking. The mechanics and calculations involved in this paper scale to involve an aerial manipulator with an adjustable number of DoF.

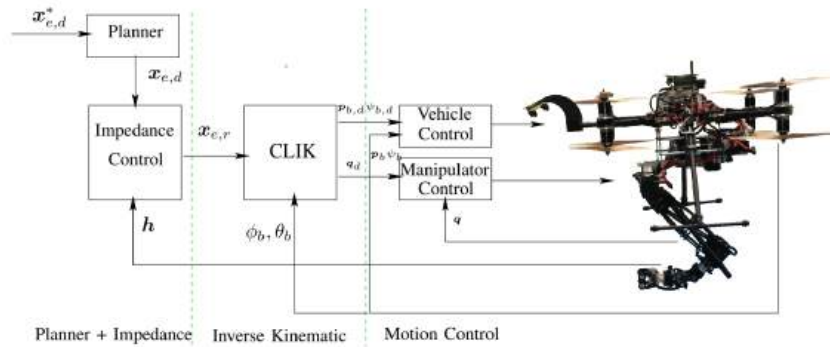


**Figure 6** Control architecture and UAV used by Cataldi et al. [12]

Ma et al. [13] introduces a novel control system designed for an aerial manipulator system, suited for a drone that shares the fixed tilt over-actuated UAV configuration used in this report. Like Ollervides-Vazquez et al. [6], a recursive Newton-Euler method was used

to acquire the dynamics model, with Kinematics based on the Craig parameter method. An Active Disturbance Rejection Control - Backstepping - Compensation (ABC) controller (Figure 7) was used to determine the exact position of the manipulator in Cartesian space. The system was simulated and the idea was theoretically proven to work, able to "achieve stable motion, position, and attitude control under the influence of the interactions between the arm and the aerial platform" [13].

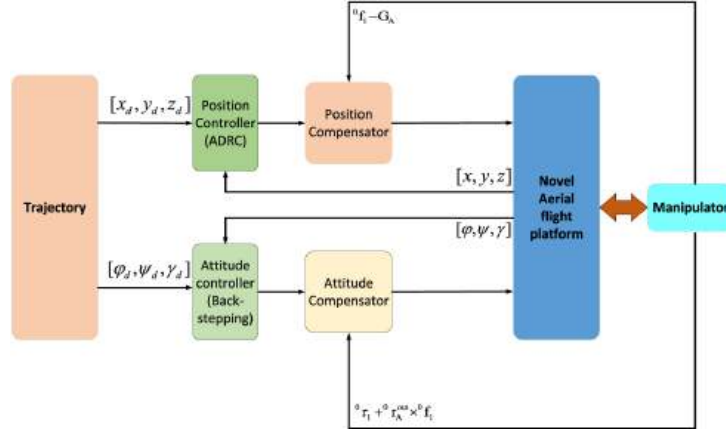


**Figure 7** Active Disturbance Rejection Control - Backstepping - Compensation (ABC) controller [13]

The control system present in the AeroX design is worth considering with manipulators on fully/over-actuated UAVs, and situations where physical interaction with a fixed environment is present. The purpose of the control system from Trujillo et al. [9] was to ensure that the drone was steady with respect to the surface of contact. The control system was made from a standard multi-rotor control architecture, modified to exploit the additional DoF of the octo-copter.

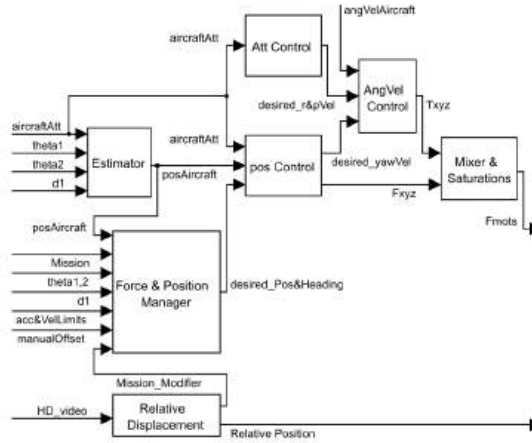


**Figure 8** Control architecture of the AeroX [9]

## 2.3 Conclusion

In the introduction and literature review, the goal of creating a drone capable of interacting with physical objects and varying the manipulator arm was introduced. The reasons behind why this would be ideal, and the potential applications were mentioned, and traditional and advanced drone designs were introduced. Articles introducing novel types of manipulator arm configurations mounted on drones were showcased, with the takeaway that drone technology has advanced to the point that manipulators with 6 DoF have been developed and patented. A few control system architectures were discussed. As a takeaway, it is seen

that traditional cascaded PID control systems modified to fit advanced setups is feasible. Numerous control systems involve a multi-layer control system architecture, largely leading to successful simulations or experimental tests. Ensuring the internal mechanisms of a manipulator produce minimal forces on the aerial body, and are accounted for in the control system is key. To this effect, ensuring the Centre of Gravity (CoG) remains as consistent as possible is of utmost importance as to ensure stability during flight.

### 3. Designs and Methods

#### 3.1 Design Considerations

##### 3.1.1 Initial UAV Specifications

A UAV was available from the beginning as a frame to make modifications to and perform experiments with. The configuration matched what the DTRG had performed previous research using: an over-actuated fixed tilt UAV with 8 rotors.

The fixed-tilt octo-rotor, hereby referable as the FT-X8 (Figure 9), was designed and optimised in a paper by Souza et al. [14]. The actuator used is the Navigator Series T-Motor MN1806 rated at KV2300. These propellers can provide a range of thrust in the range of 144G at 7.4V, 50% throttle, to 535G at 11.1V, 100% throttle.

When configured into the displayed octo-rotor setup, the angled motors drop to approximately 80% vertical capacity. With 8 propellers, this totals 3706.6 grams of maximum thrust. Without modifications, the UAV has a mass of 1157 grams, battery included.



**Figure 9** Prototype of the FT-X8 - a compact fixed-tilt octo-rotor [14]

##### 3.1.2 Initial Design Considerations

The key design consideration was to create an arm fitted onto the UAV which is capable of placing an end-effector in any position. The arm would be fitted with an interaction device with an unspecified purpose, outside of the scope of the project.

From the literature review, the AeroX design [9] stood out as the best method of including a manipulator on a UAV. Retrofitting an existing articulated joint arm robot lacked feasibility due to the price and size of such devices. The primary issue of ensuring balance was maintained led to considering designs where the arm would rotate about the centre of the UAV, akin to the first DoF included the AeroX design.

Further design considerations such as the characteristics of the motion were subject to the mechanical design, and thus were left open for change as different designs were considered.

## 3.2 Mechanical Design

### 3.2.1 Design of Rotating Mechanism

Several factors had to be considered for designing this mechanism. Ensuring the centre of mass remained fixed on the body frame during rotation was of utmost importance. Next was acquiring a full spherical range of motion to achieve the full potential of a variable arm UAV. A rotating mechanism with 180 degrees of rotation from vertically upwards to vertically downwards along with a drones ability to yaw would allow for the desired amount of freedom. However, a mechanism with the full continuous 360 degrees of rotation is ideal due to the flexibility it can provide. Side-to-side motion and general positioning of the end-effector are provided by the flight of the UAV itself. Ensuring weight was minimal was another important factor, as discussed by several of the papers in the literature review. The final factor, speed of rotation, was of low priority in comparison to the other factors due to the undefined use and speed requirements for the end-effector.

An early inspiration came from observing the motion of a planetary gear. Removing the sun gear, and instead driving one the planet gears would preserve the principle motion of a large rotating ring. The removal of the sun gear would allow for the body of the UAV to take its place. However, the configuration of the rest of the mechanism required tweaking to suit the needs of the design objectives.

An iteration of the planetary gear setup led to a design with an outward facing ring gear, and two planetary gears fixed to each other which would be able to orbit around the central gear using a motor attached to one of them. By having the motor act as a counterbalance for an arm, which would be attached to the planetary gears on the opposite side (Figure 10) However, issues with spacing and wiring become readily apparent. Mounting a motor like this would not allow it to maintain its orientation, which would require additional hardware such as a slip ring, increasing design complexity. Additionally, due to the spacing between the propellers, any object located upon a rotating ring gear could be no greater than 30 mm across, making the required orientation of the motor to drive a gear in this position unfeasible.

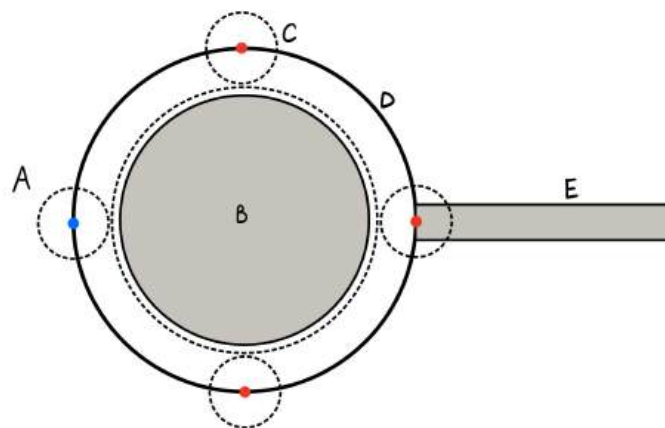


**Figure 10** Original Mechanism Design. A: Motor Driven Planet Gear, B: Body of UAV, C: Free rotating planet gear, D: Supporting Ring, E: Interaction Arm

A new design was considered which instead would have the arm attached to the ring gear.

Removing the sun gear, keeping the planet gears in fixed positions, and driving one of the planet gears with a motor circumvented the problems with the previous design (Figure 11). Although the principle of reducing weight by using the motor as a counterbalance was lost, the relative simplicity of the design, the full range of motion afforded, and the circumvention of issues of complexity made the design appealing for the initial prototyping.

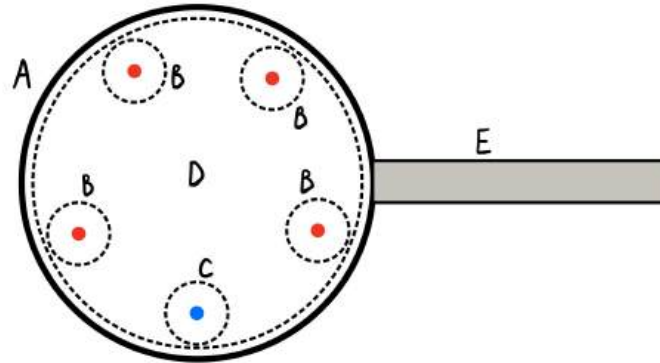


**Figure 11** Updated Mechanism Design. A: Ring Gear, B: Free rotating planet gear, C: Motor Driven Planet Gear, D: Body of UAV, E: Interaction Arm

### 3.2.2 Material and Manufacturing Method Considerations

With the weight requirements of the UAV known, and by examining existing UAVs in the drone laboratory, 3 materials become readily apparent as the optimal choices: carbon fibre, 3D printed PLA, and laser cut acrylic.

Whilst carbon fibre has the best weight-to-strength ratio of the considered materials, it is too difficult of a material to prototype with, due to the monetary and time expenses that would be incurred upon each iteration; remoulding and casting was too costly. This left 3D printing and laser cutting as the primary choices.

The frame of the UAV was elected to be laser cut due to the large and flat parts that it required. This allowed for complex 2D shapes to be designed to fit our requirements. Continuing with the previous design that was present on the provided UAV, each axis of the frame was designed as 2 parallel pieces of acrylic 11 mm apart, spaced using 3D printed hollow cylinders. This approach was used for both the leg and frame sections, and for the circular section which supported the planetary and ring gears. These 2 sections were perpendicular to each other along the vertical axis. The leg section was split into 2 halves which were designed to join to the base of the UAV, as well as to the planetary gear support using a series of 3D printed parts. The ring had an outer diameter of 210 mm, and an inner diameter 154 mm. To allow for open ended design, each acrylic frame was lined with 3 mm holes in a repeating pattern.

3D printed PLA suited the prototyping phase due to the readily available printing machines, and the ability to create tailored and complex components without complicated manufacturing techniques. Complex 3D shapes were required to support the frame, battery, and motor. Additionally, specific gear ratios were required to fit manually designed planetary and ring gear setup. The potential weight issue was circumvented by configuring the prints to use reduced infill where possible, with a higher wall count to allow for the required strength and stability in load bearing sections.

### 3.2.3 Initial Prototype Assembly

The parts for the initial prototype were developed entirely in-house, and disconnected from the UAV to allow for easier prototyping and testing. Initial print parameters for the PLA was 3 layer wall thickness with 15% infill. The initial choice of material for laser cutting was 4.5 mm clear acrylic sheets.

## 3.3 Prototype Testing and Iteration

### 3.3.1 Testing Process

A prototype was constructed using a 172:1 Metal Gear-motor 25Dx71L mm LP 6V with 48 CPR Encoder, with a Simple Motor Controller 18v7. TTL Serial communication in conjunction with an Arduino Mega 2560 was utilised to communicate with the motor controller. The motors encoder was connected to the Arduino's interrupt pin to read an angle accurate to  $0.044^\circ$ . A PID controller was attached to the input of a joystick to provide control of the motor.

Testing was performed with the frame disconnected from the body of the UAV for ease of assembly, and to prevent potential damage to the UAV. Driving the motor with a joystick successfully allowed the ring gear to rotate continuously through the full  $360^\circ$ . This result gave us confidence to move forward with the overall concept and design. Although the ring gear was still able to turn with only 2 planet gears (one driven by the motor, the other located on the opposite side to the driven gear), 4 gears were used in prototypes. This provided increased stability and decreased vibrations during rotation, and distributed the forces present on the ring gear whilst under tension more evenly.

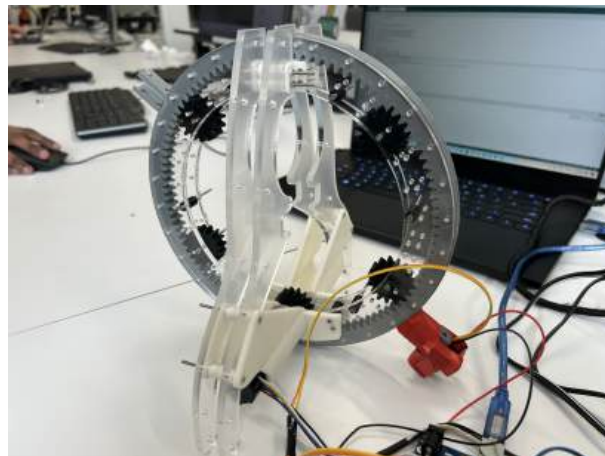


**Figure 12** Image of the original Prototype, wired to a Servo Motor

### 3.3.2 Iteration Process

Once the initial build was completed, numerous improvements were made to the structure. The frame was streamlined to be one piece rather than an adjustable structure. This simplified construction, and allowed for a more rigid joining mechanism to be built for the robotic arm as the positioning of the screw holes relative to each piece would be consistent.

The acrylic was swapped from 4.5 mm to 3 mm to reduce the weight of the laser cut frame by a third. Adjustments were made to the spacing to accommodate the change.

The ring gear was initially printed with 3 layer wall thickness and 15% infill which unfortunately did not provide the necessary structural integrity; the ring exhibited excessive

flexing and the supports for holding the arm broke after limited use. The settings were changed to a 5 layer wall thickness with 20% infill to remedy this, at the cost of an increased weight.

The prototype revealed issues with the nut and bolt combination used. 2.5 mm bolts were used to attach all components together. However, during testing, rotation of the ring gear caused the components to become loose from one another. This led to increased vibration and wear. The solution was nylon locking nuts, commonplace in hobbyist UAV builds. These ensure that components such as the propellers do not come loose during continuous rotation and vibration.

The requirement for two additional micro-controllers to be implemented to drive a servo motor, along with its unwieldy shape gave rise to the idea to use a motor type more inherently compatible with the PixHawk. From previous research conducted at the University, a Dynamixel was recommended. We acquired an MX-106 Dynamixel. The X series of this motor all follow the same chassis design, which allows for the potential to swap out the motor model in use if the requirements change. Although ultimately heavier, the ability to directly interface with the PixHawk, and the much higher torque capabilities of this new motor were capable of streamlining the control systems section of the project, as complex serial communication or torque increasing gear ratios would not be required.



**Figure 13** CAD model of the updated prototype, containing 3D models for printing and parts for laser cutting

### 3.3.3 Finalised Physical Prototype

Using everything that had been iterated upon and improved, a final iteration of the UAV was completed. The Dynamixel motor was designed to act as a support between the ring gear frame and the leg. The battery was offset from the centre of the geometry in the opposite direction to the motor. A support between the ring gear frame and legs was created to support the battery, with a slot system to allow for a strap to hold the battery firmly in a range positions to allow for fine tuning of the balance. The payload of the modified UAV came out to be 1411 grams with the Dynamixel and a carbon rod for an end-effector attached. With a battery mass of 375 grams the total flight payload came to 1786 grams without an end-effector.

To adjust the play between the ring and planet gears, the motor mount was adjusted by reprinting with alterations to the vertical position of the shaft. This was iterated until a

smooth low resistance rotation was achieved.

With the arm detached, and motor shaft disconnected to allow for potential rotation of the mechanism, the UAV was flight tested. The test showed that the UAV was capable of liftoff, and remained balanced with even loose positioning of the battery.



**Figure 14** UAV Prototype utilised in experiments

### **3.4 Actuator and Code Design**

#### *3.4.1 Dynamixel Setup*

Using the previous work of Pedro Mendez, the setup process of the Dynamixel was streamlined as it was possible to utilise an existing PX4 code and Simulink base. Establishing control of a Dynamixel motor requires the motor to be powered by an appropriate voltage source and a physical wire connection utilising TTL Serial communication with a correct baud rate.

During flight, the battery can drain from 12.5V to 8V if the motors become over-saturated from high physical loads or unaccounted physical interaction. A voltage regulator was used to ensure the variation in voltage did not directly effect the performance of the Dynamixel or cause inadvertent damage, by continuously supplying 12V.

Utilising a USB connection, the Dynamixel was connected to a computer loaded with the Dynamixel Wizard software: official software designated to directly control the motor and view the status of each address. The software allowed for the identification of the ID and baud rate the motor utilised - a factor prone to variation between each Dynamixel. The Dynamixel Wizard utilises a scanning method to identify available motors which could be circumvented if the connection specifications of a motor was known.

The control of a Dynamixel is handled through a series of addresses, each storing variables relating to its control and status. Variables such as operating mode, current encoder position, control set-point, torque-enable, and even temperature can be read and, if appropriate, written to. The operating mode refers to how a given set-point will be used. Velocity mode infers the set-point as a target velocity, whereas position control modes view it as

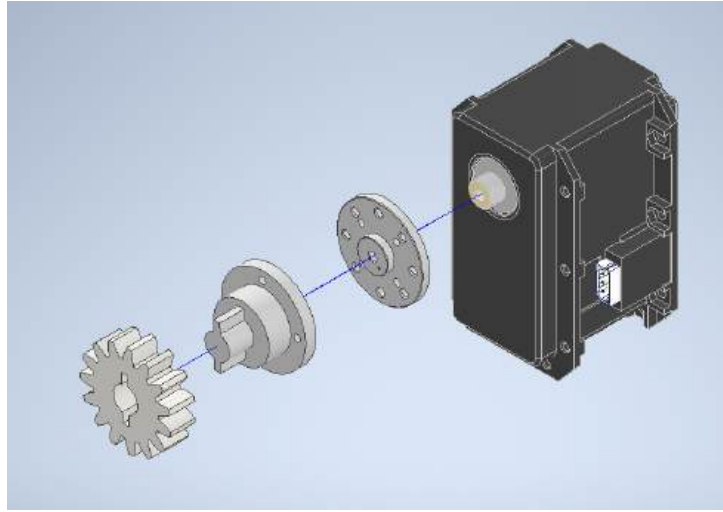


**Figure 15** Shaft coupling between Dynamixel and rotating mechanism

an encoder position to target. Switching operating mode requires Torque-Enable to be off, whilst driving the motor requires Torque-Enable to be on. Once the connection to the Dynamixel is established, and the operating mode has been correctly acquired following the Torque-Enable requirements, sending a set-point is all that is required to control the motor. The internal micro-controller responsible for establishing communications also contains a PID control system to handle actuation beyond this point. This internal control system further impresses the usefulness of utilising Dynamixel for UAV applications, as it reduces the computation requirements the flight control must undergo at any given moment.

Utilising knowledge of the addresses, the ID, and the baud rate, the PixHawk is capable of performing communication with the Dynamixel. A custom module named *dynamixel\_serial* was available which handled the higher-level aspects of communication, such as the initialisation of the connection by directly using the the correct baud rate and ID. This module was also responsible for printing Dynamixel related messages, troubleshooting through the UAV console, and setting the desired set-point received from the MAVLink.

An internal lower level module labelled *Dynamixel\_Protocol* was responsible for handling the factors such as the addresses, preparing data bits to be sent through the serial, and switching operating mode. Once a control input was sent from the higher level the internal module handled the raw, direct communication aspects.

### 3.4.2 Off-board Simulink Control

In order to control the UAVs flight systems and actuated arm the Motion Capture Lab was used. The Motion Capture Lab contained various systems vital for control and analysis of the of the UAV. This included a Vicon camera system capable of tracking high-visibility light-reflecting balls attached to objects, and a MATLAB-Simulink system designed for controlling aspects of the UAV such as its positional set-points on a inertial frame, and individual velocities for all 6 axis of the UAV. The Vicon object tracking system is capable of feeding the positional data of objects into the Simulink system. The Simulink can organise data into a User Datagram Protocol (UDP) to be sent through the MAVLink, hosted on an ESP32 WiFi module connected to the one of the PixHawk 4s physical inputs. By sending control input containing a desired X, Y, and Z position, a yaw of  $-\pi/2$ , and axis velocity set-points of 0, a UAV can informed to target a position in space and attempt to hover, seen in Figure 16.

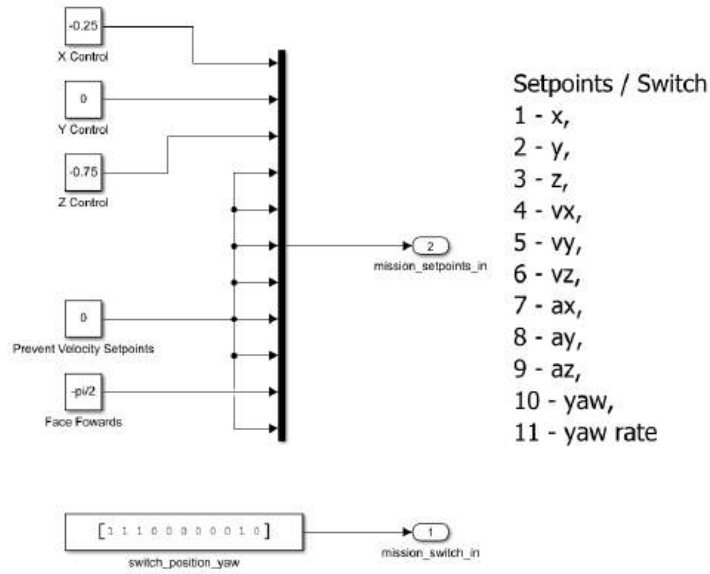


**Figure 16** Position and velocity control variables being organised

In addition to a message containing desired set-points for positional control, a message labelled *Debug Vect* is sent through the MAVLink. The *Debug Vect* holds 3 value flags, named x, y and z for miscellaneous information sending. The Dynamixel serial module is initialised to read the *Debug Vect* message, and parse the x value into a set-point for the motor. The received integer is multiplied by 4095 making each increment in value correspond to one full revolution of the motor.

### 3.4.3 Dynamixel Troubleshooting

Unfortunately, before the Dynamixel could be utilised in experimental testing, a series of troubleshooting steps had to be taken before it would correctly work. Once the wiring was completed, it was realised that the initialisation protocol was defaulting to an incorrect baud rate and ID, leading to a failure to communicate.

Testing the Dynamixel with the Wizard application in an effort to acquire the correct communication protocol information revealed further issues. For unclear reasons the Dynamixel was unable to undergo any form of position control. Encoder reading, and velocity control worked as expected yet attempts to change to change the desired encoder position would lead to timeout errors.

Ultimately, the issues were fixed by switching to a new Dynamixel motor from the same series - the Dynamixel MX-64T. The only differences were a lower mass of 135 grams, and a marginally decreased torque profile, remaining well within the requirements for operating the mechanism. Undergoing similar checks to ensure that the communication was initialising correctly and connecting the Simulink setup resulted in successful control.

### 3.4.4 Validating Flight System

The *Debug Vect* consists of float32 variables. In an attempt to increase the resolution of the arm position control, debug messages containing float variables corresponding to  $15^\circ$  increments of the arm were used. The existing setup used integer values, each rotating the Dynamixel one full revolution. Equation 1 calculates  $i$ , the value needed to be input into

the *Debug Vect* to acquire a desired angle,  $\theta_{\text{Desired}}$ . This includes the gear ratio of  $\alpha:1$  present between the motor and the gear the arm is attached to.

$$i = 1 + \theta_{\text{Desired}} * \frac{\alpha}{360} \quad (1)$$

To make this change, a dial on the Simulink was updated to contain each value, calculated from Equation 1 with increments of  $15^\circ$ , to create a full  $360^\circ$ . Updating the MAVLink with the UAV grounded showed that the update worked correctly, allowing the actuated arm to target the smaller increments. However, issues quickly arose. Reading the logged output with the updated dial revealed that the new *Debug Vect* was not correctly showcasing the changes, defaulting to 0 despite the viewed, successful arm motion. More pressingly, the set-point tracking of the UAV during flight greatly suffered, becoming unable to reach a stationary point despite no imbalances in the physical geometry of the UAV. Reverting the change in the dial to send pure integers fixed the issue, despite no direct overlap in the systems at play. It was suspected that the Simulink was not correctly initialised to send floats over the MAVLink system leading to telemetry lag physically manifesting in a slowed control system and an inability to update the rotors control inputs in real-time. However, for the purposes of time, these issues were not further investigated and instead the arm position dial was reverting to the integer setup with angle set-points in increments of  $51.4^\circ$  as seen in Figure 17.

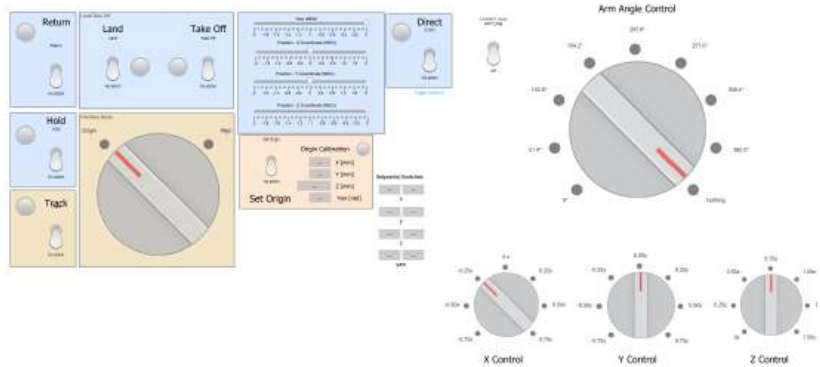


**Figure 17** Off-board high-level view of Simulink controller, including an arm position dial

Another way the arm position resolution was attempted to be increased was through the PX4 code build itself. The current parameters were saved to maintain prior tuning on the FX-8T. Using the GitHub build stated to be present on the UAV according to recent logs, the *Debug Vect* flag multiplication was altered from 4095 to 1194.

$$4095 * \frac{7}{1} * \frac{15}{360} = 1194.375$$

However, further issues appeared when attempting to build the code after alteration. Following the PX4 developer guide and building the GitHub recursively into an Ubuntu environment proved unsuccessful. The root cause of the issue appeared to be that the Dynamixel compatible build of the PX4 code was outdated and any attempt to build it would use update-to-date versions of relevant modules leading to issues during the build. For the same reasons as the attempts to fix the *Debug Vect*, this approach was scrapped and it was decided that a positional resolution of  $51.4^\circ$  would suffice for testing.

## 4. Experiments and Data Processing

### 4.1 Experiment Setup and Process

It was decided that testing how the movement and weight present on the arm at a fixed distance would affect the overall flight and stability of the system. Adjusting the weight incrementally would shift the CoG further from the UAVs centre of geometry and rotation. Investigation of the relation between movement of the arm, difference between the centre of rotation and the CoG, and a few different metrics of error in UAV stability would reveal characteristics about the performance of the UAV, potentially shedding light on the feasibility of the arm mechanism and required future steps.

Each experiment was conducted by incrementing the weight on the end of the carbon rod attached to the rotating carbon rod by 20 g. The weight was attached at a fixed distance of 245.7 mm. It was tested to see if the UAV was capable of achieving stable position control. Piloting the UAV with the transmitter in Manual Control Mode, the UAV was manoeuvred into a physical position close to the off-board set-points. Next, the transmitter was switched to off-board control mode, passing control from the pilot to the Simulink system, where the UAV would attempt to acquire the position set-points and settle. Once visually stable, the arm was actuated a full rotation in both directions.

As the flight log of the UAV did not record the current encoder reading, the Vicon system was used to track the relative rotation of the arm to the body. To ensure the information recording by the Vicon was accurate, the tracking objects were created to ensure their origins were perfectly aligned when the arm was set at a horizontal position. This origin point was set at the centre of rotation of both the UAV and the arm mechanism. Doing this ensured that tracking the position of the UAV or the arm would plot the same path, allowing for an additional form of tracking vibration. The more important metric, rotational recordings, would remain the same no matter the location of the origin.

During each experiment, a couple of recording devices were set up facing the UAV to allow for a visual recap. The Vicon system was set to record the movements of the tracked objects. Once finished recording, the Vicon could export the relevant data as a .csv file. Each flight of the UAV between arming and disarming saved a log contained a stack of recording data such as set-points, rotor thrusts, battery levels and pitch. Each log could be downloaded and parsed through a dedicated PixHawk flight review website, or read using a MATLAB add-on.

### 4.2 Issues Faced During Experimentation

#### 4.2.1 Weight Limits

With the weight of the UAV nearing the allowable limit to ensure flight was possible, the weights of the counterbalance and end-effector had to be kept to a minimum. An initial attempt to fly the UAV with the full OmhStick end-effector and a counterbalance was too heavy of an addition to the payload, and prevented the UAV from being able ascend at a reasonable rate, significantly limiting the possible movement and over saturating the motors resulting in rapid battery loss.

The main weight factor in the initial unsuccessful flight test was the counter balance. With torque as a trade off between distance and weight, any attempt to reduce the physical geometry of the UAV resulted in a counter balance too heavy too allow for flight.

It was found that removing the counter balance, and flying the OmhStick was achievable, hence adjusting the range of experiments possible, and providing the limits for physical testing.

#### 4.2.2 *Flight Control*

It was during initial experimentation where the issues surrounding an attempted increase of position control resolution came to light. During the flights effected by this the experimentation steps after switching to off-board control mode were unfeasible due to the lack of stability, battery drainage, and rotor actuator saturation.

#### 4.2.3 *Battery Drainage and Actuator Saturation*

Between each test a device was used to check the battery level of the UAV ensuring it remained above 11.1V. From full charge of 12.5V each standard flight, lasting roughly 4 minutes, typically drained half of a volt. However various factors could alter this rate.

Over-saturation of the rotor actuators occurred when the UAV attempted non-feasible flight manoeuvres, particularly when its mass approached the maximum allowable flight load. Another situation contributing to excessive battery drain involved unstable flight conditions, where the UAV applied large control gains to recover from significant position errors.

Both scenarios were encountered during initial flight testing, resulting in rapid battery depletion and underscoring the importance of thorough pre-flight checks.

### 4.3 **Parsing of Data**

#### 4.3.1 *Data Logs*

Using a series of MATLAB scripts the data was extracted and parsed for visualisation and analysis. Each useful log was downloaded via a USB connection the UAV and initially passed into the PX4 Flight Review website, a dedicated location to conveniently view the broad statistics about the flight. This included factors such as positions acquired against set-points, pitch error, battery levels, actuator usage, transmitter control mode, and kill-switch activation. The flight review acted as a way to quickly visualise the data and troubleshoot issues as needed.

For statistical analysis of the data, the MATLAB add-on 'UAV Toolbox' was downloaded providing a dedicated function for reading uLog files. All of the raw data recorded from the .msg file, such as everything mentioned in the Flight Review section and more such as the *Debug Vect*, is available whilst using this function.

#### 4.3.2 *Vicon Data*

The data containing the translation and rotation of the two tracked objects was exported from the Vicon software as a .csv file. The files were exported into MATLAB and converted into real time using the FPS of the cameras of approximately 100, where each row of data corresponded to 1/100th of a second.

#### 4.3.3 *Overlaying Data*

The key piece of information from the Vicon recording was the rotation of the arm. The rest of the information for analysis was stored on the logs. However, the time-frames inherent to each information storage base were uncoupled, hence requiring manual overlaying of

data. To do this, the relative rotation of the arm was plotted. This was calculated by subtracting the rotation of the arm from the rotation of the body in each individual axis, then performing the Pythagorean equation to extract the total relative rotation as seen in Equation 2.

$$\theta_{Arm} = \sqrt{(\theta_{xBody} - \theta_{xArm})^2 + (\theta_{yBody} - \theta_{yArm})^2 + (\theta_{zBody} - \theta_{zArm})^2} \quad (2)$$

The total relative rotation mathematically represented the angle of the arm relative to the body. During a flight where the arm was set to remain horizontal, performing this calculation removes the pitch, yaw, and roll undergone by the body of the UAV and reads as  $0^\circ$ .

Overlaying the total relative rotation of the arm with the *Debug Vect* commands sent to the arm, after converting the integer value into it's representative angle, allows for the actual vs desired arm angle to be plotted. By adjusting the slice of time being displayed on the log and Vicon data, they could be overlaid.

As a final check to make sure all the data could be correctly used during statistical analysis and plotting, the largest data array was used as a base array. The rest of the data was linearly interpolated against the base array to create a functionally identical data array. This allowed for direct comparisons of points in time, as well as ensuring compatibility for statistical analysis functions to be performed between any given sets of information.

## 5. Results and Discussion

### 5.1 No End-Effector Mass Installed

The initial and longest experiment included a run with no end-effector installed, nor any mass to simulate one. The carbon fibre rod was kept attached during this run to account for it's presence during future runs. Additionally, it was of interest to see if the geometric presence of the rod would have any significant effects.

During this test it was found that the UAV had little issue stabilising after the switch from manual control to off-board position control. After some broad position oscillation the UAV quickly settled into a position with less than 5cm deviation for all 3 axis. This was quickly deemed as visually stable enough to perform the arm movements. During this test, the arm was rotated to each available position through the 7 integer range, in order to view if particular angles would have adverse effects on general stability.

Once the full range was completed in both clockwise and anticlockwise directions, the arm was sent on a full rotation forwards and backwards. This was done as to ensure the no-mass test contained the same motion which was to be undergone during future tests. Once again, full stability was maintained.

Although the the graph in Figure 18 implies the angles were not correctly acquired, in practice they were. The increasing offset angle can be attributed to measuring errors with the Vicon setting gradually increasing as the arm rotated, and correcting once the arm had completed one full revolution. A repeat of this test may correct this, as the Vicon system had previously proven capable of accurately calculating the angle of the arm.

By considered the X, Y, and Z position tracking plots in Figure 19 it can be seen that the

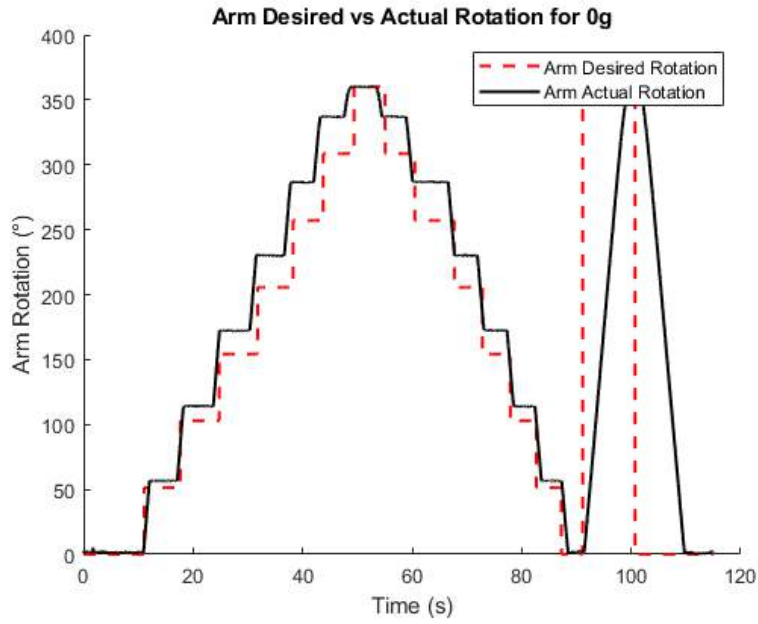


**Figure 18** Plot of the actuated arms angular set-point tracking with no end-effector attached

X, Y and Z positions do deviate more than 5cm from the desired set-points throughout the full duration, which is plotted across a 2 minute time period involving movements of the arm.

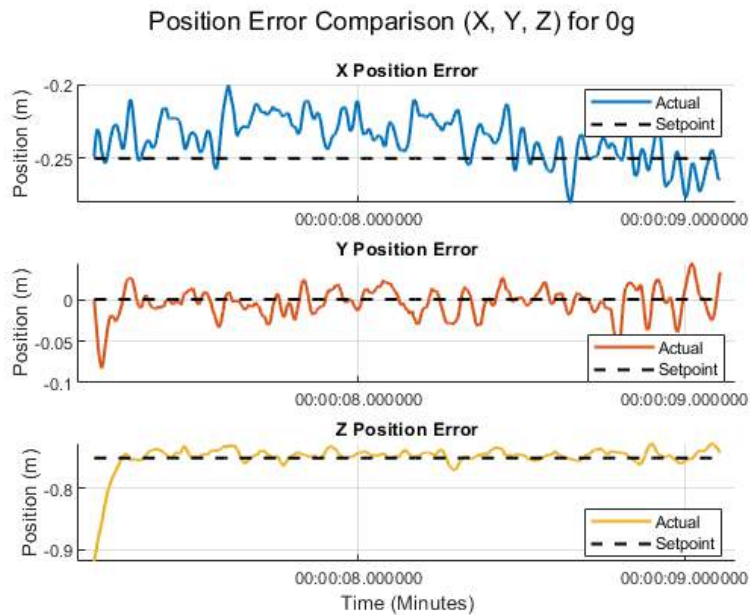


**Figure 19** Plot of the UAVs set point tracking with with no end-effector attached

In order to acquire the angular velocity of the arm the relative arm position was differentiated, then smoothed. The smoothing was done using a moving window average with a size of 100, and then passed over with a low-pass filter with a cutoff frequency of 1Hz in order to ignore the inaccuracies of the Vicon system or vibrations present on the reflective balls. The result was a smooth velocity function that accurately showcased the movement of the arm. Taking the absolute of this and comparing it to the absolute pitch error of the UAV across the same time frame revealed a loss correlation with an R value of 0.3578. Although indicative of a relationship, it could not be considered significant enough to draw

any conclusions.

## 5.2 Increasing Mass Installed on End-Effector

The next 3 experiments conducted applied the increasing weights on the end-effector as discussed in Section 4.1. It was quickly noticed that as the mass increased the overall stability of the UAV dropped, taking longer to settle after engaging off-board control, and having larger deviations in position whilst in this mode as seen by the plot in Figure 20.

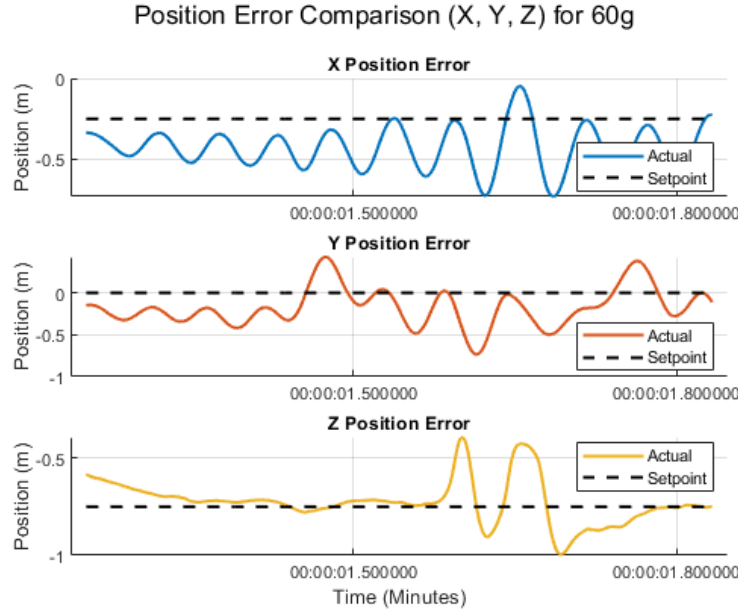


**Figure 20** Plot of the UAVs set point tracking with 60g attached to the arm

It was seen that driving the arm actuator in this mode resulted in more significant pitch variation, resulting in further destabilisation of the UAV. However, the degree of destabilisation encountered was never too large as to cause loss of flight control. The relation between pitch error and angular velocity as seen in Figure 21 provides insight as to how the the pitching of the UAV is prone to significant rise during arm motion.

Significant Flight Error Metrics				
Mass (g)	0	20	40	60
Max Pitch Error (°)	0.7497	1.4617	1.7806	2.9808
Max X Error (cm)	4.9425	85.0771	47.1759	48.0625
Max Y Error (cm)	8.2705	69.6064	76.3593	73.3155
Max Z Error (cm)	2.4361	7.3168	34.5359	35.7603
Pitch vs Velocity R Value	0.35758	0.3761	0.6397	0.72646

The angle control of the arm was not effected by mass as the mechanical attributes of the system are inherently uncoupled. Seen in Figure 22 the rotation of the arm undergoes a smooth motion accurately targeting the desired angle.

By comparing the correlation between the absolute pitch error and the absolute velocity of the arm it is seen that increasing mass leads to a greater correlation. This was clear both visually as seen by the increase in pitch movement whilst the arm moved, and statistically as seen by the R value increasing with mass in Figure 23.

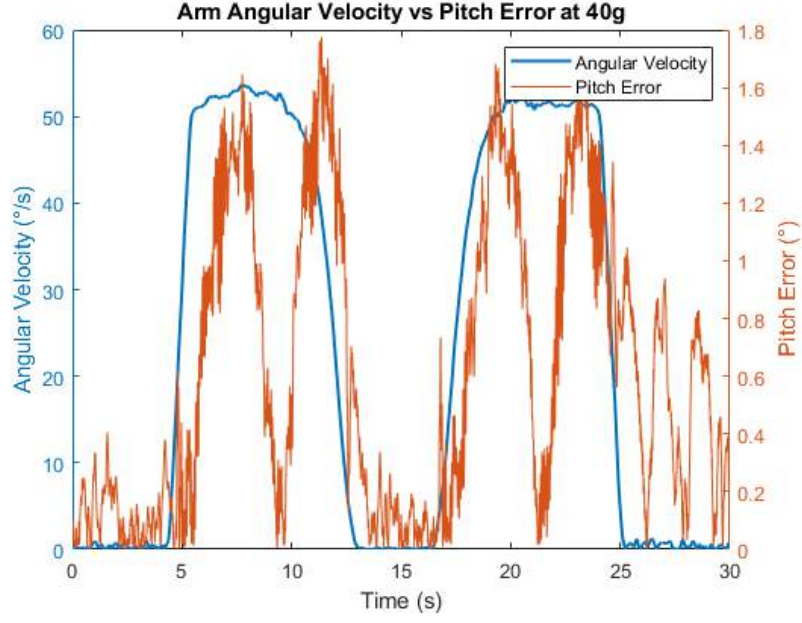


**Figure 21** Plot of the Pitching error against the velocity of the arm with 40g attached to the arm

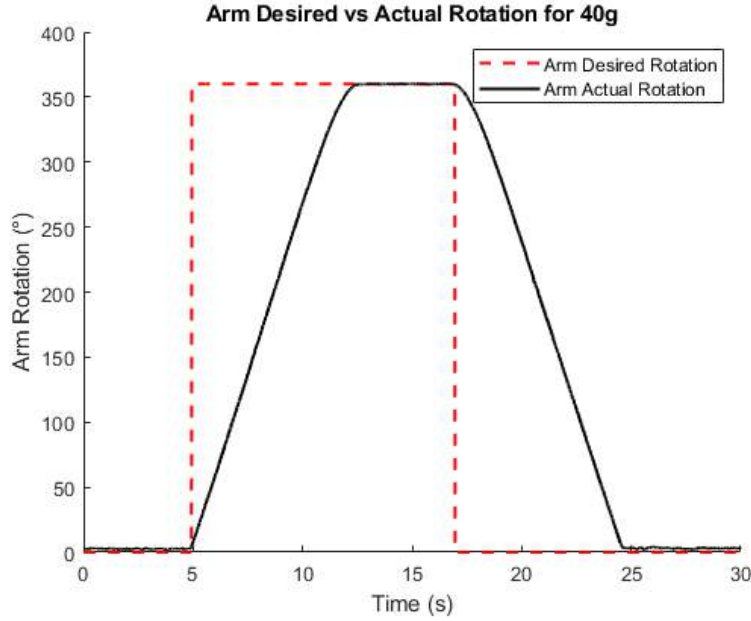


**Figure 22** Plot of the actuated arms angular set-point tracking with 40g attached to the arm

Beyond a value of 0.6, the correlation coefficient can be considered approaching a high level of statistical significance. As a conclusion this reveals that regardless of the mass imbalance experienced across the centrally rotating arm actuator, a correlation between arm velocity and angular pitch error can be observed. As this mass imbalance becomes greater, movement of the arm results in larger and more significant pitch error.

Considering the deviation in error experienced across increasing masses showcases worsening standard deviations as seen in Figure 24. Performing linear regression for the errors showcases a positive relation between the weight and error. In the tested range the positional error becomes 4.5 cm worse and the pitch error becomes  $0.288^\circ$  worse for every 20 g added or for every 2.7 cm the CoG deviates from the centre of the UAV. This is found by balancing the moments with the torque equation  $\tau = M \cdot d$ , seen in Equation 3.

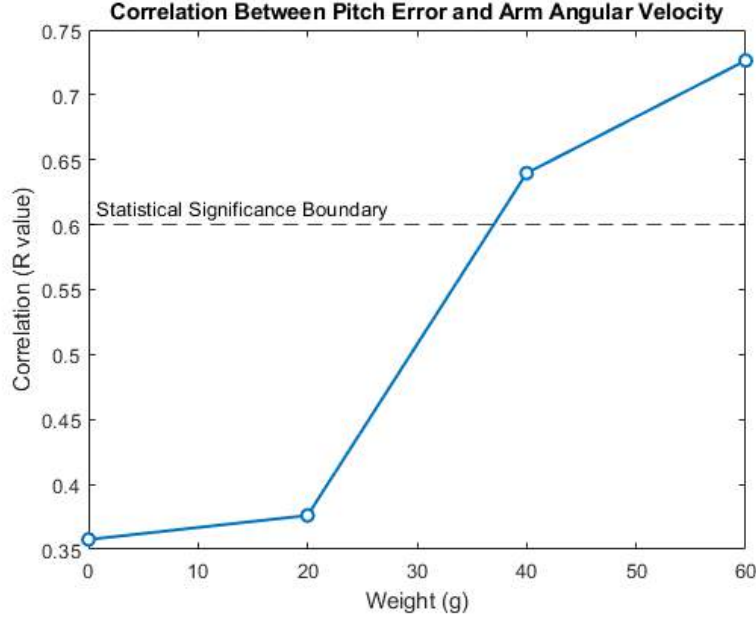


**Figure 23** Plot of the actuated arms angular set-point tracking with 60g attached to the arm

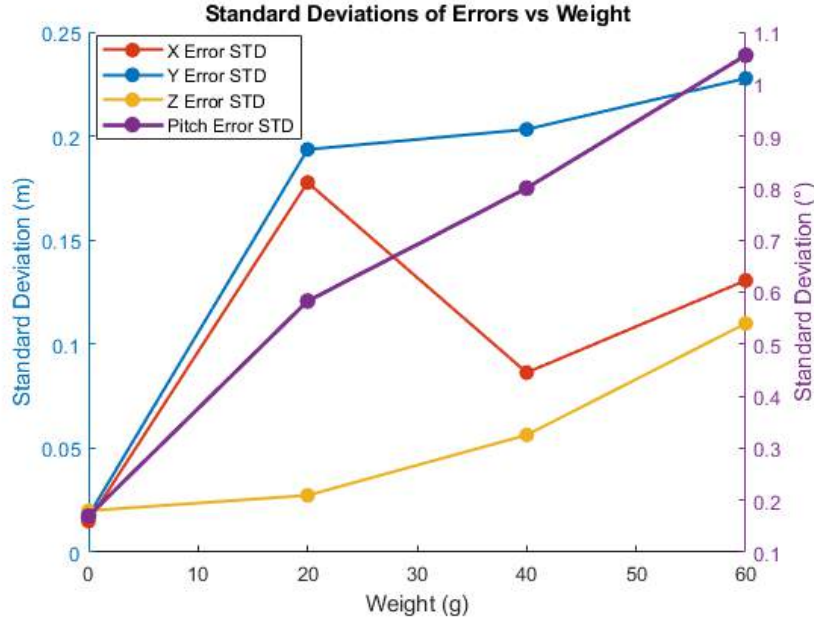


**Figure 24** Plot of the Standard Deviation of Errors against weight for X, Y, Z and Pitch control of the UAV body

$d_{\text{End-Effector}}$  refers to the distance of the end-effector from the centre of the UAV and  $\Delta d_{\text{CoG}}$  refers to the change in distance of the CoG.

$$\Delta d_{\text{CoG}} = \frac{M_{\text{End-Effector}} \cdot d_{\text{End-Effector}}}{M_{\text{UAV}} + M_{\text{End-Effector}}} \quad (3)$$

As seen in Figure 24 with no weight attached the error metrics are low, averaging 2cm of position deviation and  $0.2^\circ$  of pitch deviation. However, as mass is attached to the end-effector the error in the X, Y, and Pitch quickly rise. Considering the simplified mechanics

Element	Equation
X	$y = 0.0013x + 0.0641$
Y	$y = 0.0032x + 0.0645$
Z	$y = 0.0015x + 0.0085$
Pitch	$y = 0.0144x + 0.2208$

**Table 1** Linear Regression Equations

of the system as a beam lever with a pivot point located in the centre of the propellers as in Figure 25, the addition of the weight acts as a destabilising force, if no counterbalance is included, removing the balance of the system. The control system of the UAV is forced to compensate for this and successfully does so, yet the pitching error can be attributed to this inherent imbalance.

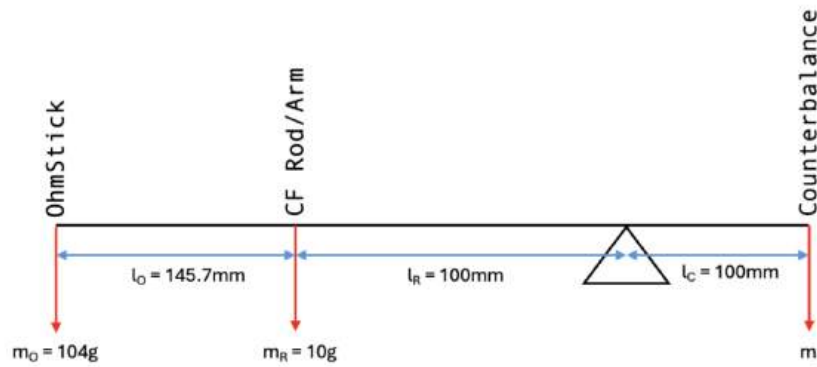


**Figure 25** Model of UAV and Actuated arm system as pivoting lever

As the arm rotates, the CoG moves in a circular motion about the centre of the UAV body. The movement of the arm and CoG correspond to increased pitching errors. This relationship grows stronger as end-effector mass increases, as seen in Figure 23, demonstrating that the relative position of the CoG to the body of the UAV has a direct effect on its ability to maintain stability in the axis of CoG rotation.

Any errors in pitch can directly lead to deviation in X and Y positioning as the pitch controls the position of the UAV most significantly along these axis. The vertical, or Z, control of the UAV can remain relatively stable. As the mass increases the Z error continues a gradual upwards trend as seen in Table 1, likely due to factors such as actuator saturation limiting the UAVs ability to maintain flight.

### 5.3 OhmStick Installed on End-Effector

The final test performed was with an attached OhmStick, and a flight test was conducted in accordance with the previous flight tests.

During take-off and manual flight control the UAV remained stable, with high amounts of vibration visible on external components. Once off-board position control mode was engaged the UAV rapidly lost stability as the actuators saturated due to high position errors and large control inputs. As the UAV attempted to regain stability by pitching, the flight stability became critical as it attempted to flip. The kill-switch was activated quickly, allowing the tether to protect the UAV from physical as it fell.

The pitch angular rate as seen in Figure 27 showcases the vibration of the UAV during

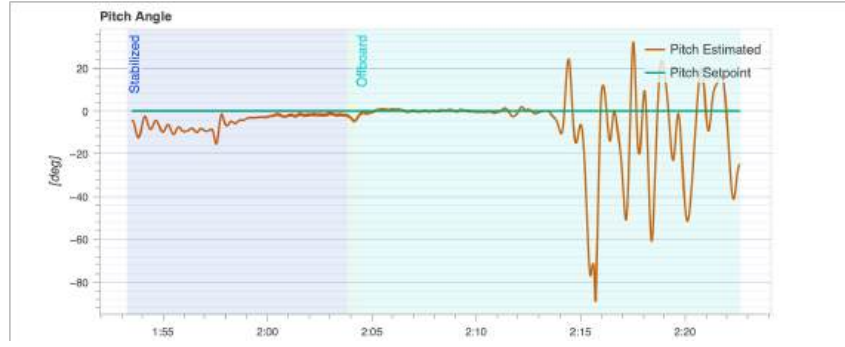


**Figure 26** Pitch Angle during attempted flight with OhmStick attached

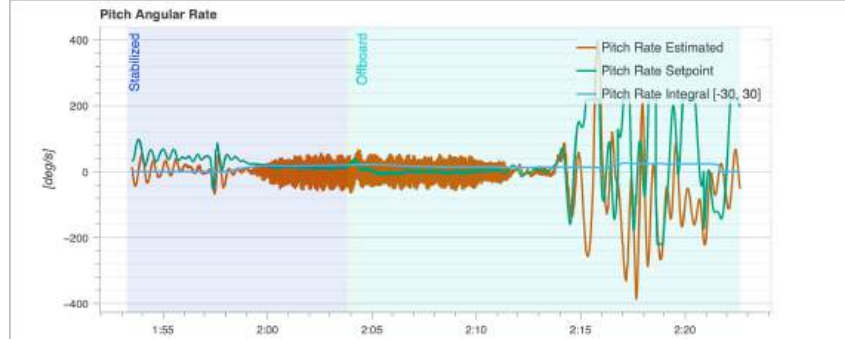


**Figure 27** Pitch Angular Rate during attempted flight with OhmStick attached

this attempted flight. A high degree of oscillation can be seen even before off-board mode is engaged, indicative of an potentially unstable flight. This increase in vibration can be associated with an increase in weight and is consistent in findings from other studies such as Ge et al. [15].

Altering the angle of the arm to be vertical in an attempt to bring the CoG to be inline with the centre of rotation worsened the effects of vibration. Before take-off had completed the amount of vibration occurring was already greater than what was seen in prior flights, leading to an early cancellation of this flight test.

## 6. Conclusions and Future Works

### 6.1 Conclusions

In conclusion, although time did not permit contact testing and flight controller modification of the UAV, the physical modifications performed to the UAV and experiments performed proved insightful in the area of actuated end-effectors attached to UAVs. Various mechanisms were considered before an actuator capable of maintaining flight stability was designed, manufactured, physically implemented and tested.

Despite no flight controller modifications being made, the ability for the UAV to remain stable whilst manoeuvring the arm and controlling for position was notable,

The addition of weights ranging up to 60g without the inclusion of a counterbalance was experimentally investigated to reveal the range of potential flights, and hints at the potential for weight reduction by way of omission of a full counter balance.

The relation between velocity of pitch error gives rise to the notion of decreasing the maximum velocity of the arm actuation to increase the stability during arm manoeuvring.

Due to limitations in the maximum allowable flight payload of the UAV, the method used to increment the weight of the end-effectors contains a few unaccounted variables. It becomes unclear what the direct cause of the increase in error deviation is when considering it could be from the greater weight of the overall UAV present on the end-effector, or the new position of the CoG.

## 6.2 Future Works

For future work, there is significant potential for the continuation of the project. Further weight reductions or increase in rotor thrust could be attempted to increase maximum allowable payload of the UAV, and in turn allow for a heavier end-effector and counterbalance system. Testing the actuation with a counterbalance in place would reveal more about the effects of increasing mass whilst keeping the CoG in a singular position.

Work could be done to reduce the vibrations present in the system such vibration dampers or a more stable joining mechanism between the carbon fibre rod and the rotating mechanism.

Once complete, experimentation could be done to test physical contact between the UAV and a grounded object such as a mock power line. Further tests could be done to investigate how movement of the arm effects stability whilst interaction is occurring.

Finally, a pipeline ensuring complete connection between elements of the motor and the PixHawk code could be developed. Allowing for the encoder value of the motor to be access by the flight controller rather than by analysing a Vicon recording would allow for use of the UAV outside of the the Motion Capture Lab, and for the velocity and angle readings of the actuated arm to be used in potential modifications to the control system.

## References

- [1] V. Kangunde, R. S. Jamisola Jr, and E. K. Theophilus, "A review on drones controlled in real-time," *International journal of dynamics and control*, vol. 9, no. 4, pp. 1832–1846, 2021.
- [2] G. Mahajan, "Applications of drone technology in construction industry: A study 2012-2021," *International Journal of Engineering and Advanced Technology*, vol. 11, no. 1, pp. 224–239, 2021.
- [3] S. Ahirwar, R. Swarnkar, S. Bhukya, and G. Namwade, "Application of drone in agriculture," *International Journal of Current Microbiology and Applied Sciences*, vol. 8, no. 01, pp. 2500–2505, 2019.
- [4] K. Chan, "Drone flight control for contact testing of power lines," *Department of Mechanical and Mechatronics Engineering The University of Auckland*, no. 1, p. 23, 2023.
- [5] P. Wegrowski, W. Thomas, J. Lemrick, and T. Deemyad, "Advanced folding robotic arm for quadcopters," in *2022 Intermountain Engineering, Technology and Computing (IETC)*. IEEE, 2022, pp. 1–6.
- [6] E. J. Ollervides-Vazquez, P. A. Tellez-Belkotosky, V. Santibañez, E. G. Rojo-Rodriguez, L. A. Reyes-Osorio, and O. Garcia-Salazar, "Modeling and simulation of an octorotor uav with manipulator arm," *Drones*, vol. 7, no. 3, p. 168, 2023.

- [7] B. Suthar and S. Jung, “Design and feasibility analysis of a foldable robot arm for drones using a twisted string actuator: Frad-tsa,” *IEEE Robotics and Automation Letters*, vol. 6, no. 3, pp. 5769–5775, 2021.
- [8] A. Ollero, G. Heredia, A. Franchi, G. Antonelli, K. Kondak, A. Sanfeliu, A. Viguria, J. R. Martínez-de Dios, F. Pierri, J. Cortés *et al.*, “The aeroarms project: Aerial robots with advanced manipulation capabilities for inspection and maintenance,” *IEEE Robotics & Automation Magazine*, vol. 25, no. 4, pp. 12–23, 2018.
- [9] M. Á. Trujillo, J. R. Martínez-de Dios, C. Martín, A. Viguria, and A. Ollero, “Novel aerial manipulator for accurate and robust industrial ndt contact inspection: A new tool for the oil and gas inspection industry,” *Sensors*, vol. 19, no. 6, p. 1305, 2019.
- [10] G. Muscio, F. Pierri, M. A. Trujillo, E. Cataldi, G. Giglio, G. Antonelli, F. Caccavale, A. Viguria, S. Chiaverini, and A. Ollero, “Experiments on coordinated motion of aerial robotic manipulators,” in *2016 IEEE international conference on robotics and automation (ICRA)*. IEEE, 2016, pp. 1224–1229.
- [11] F. Ruggiero, M. A. Trujillo, R. Cano, H. Ascorbe, A. Viguria, C. Pérez, V. Lippiello, A. Ollero, and B. Siciliano, “A multilayer control for multirotor uavs equipped with a servo robot arm,” in *2015 IEEE international conference on robotics and automation (ICRA)*. IEEE, 2015, pp. 4014–4020.
- [12] E. Cataldi, G. Muscio, M. A. Trujillo, Y. Rodríguez, F. Pierri, G. Antonelli, F. Caccavale, A. Viguria, S. Chiaverini, and A. Ollero, “Impedance control of an aerial-manipulator: Preliminary results,” in *2016 IEEE/RSJ International Conference on Intelligent Robots and Systems (IROS)*. IEEE, 2016, pp. 3848–3853.
- [13] L. Ma, Y. Yan, Z. Li, and J. Liu, “A novel aerial manipulator system compensation control based on adrc and backstepping,” *Scientific Reports*, vol. 11, no. 1, p. 22324, 2021.
- [14] P. H. M. Souza, “Dynamics and control of unmanned aerial vehicles for prolonged interaction with compliant environments,” in *NA*. The University of Auckland, 2023, p. 135.
- [15] C. Ge, K. Dunno, M. A. Singh, L. Yuan, and L.-X. Lu, “Development of a drone’s vibration, shock, and atmospheric profiles,” *Applied Sciences*, vol. 11, no. 11, p. 5176, 6 2021. [Online]. Available: <https://www.mdpi.com/2076-3417/11/11/5176>